Psammomatoid Ossifying Fibroma Is Defined by SATB2 Rearrangement

Cleven, Arjen H.G.; Szuhai, Karoly; van IJzendoorn, David G.P.; Groen, Eline; Baelde, Hans; Schreuder, Willem H.; Briaire-de Bruijn, Inge H.; van der Meeren, Stijn W.; Kleijwegt, Maarten C.; Furth, Wouter R.

Published in:
Modern pathology : an official journal of the United States and Canadian Academy of Pathology, Inc

DOI:
10.1016/j.modpat.2022.100013

Mod Pathol 36 (2023) 100013

MODERN PATHOLOGY

USCAP UNITED STATES AND CANADIAN ACADEMY OF PATHOLOGY
Creating a Better Pathologist

Journal homepage: https://modernpathology.org/

Research Article

Psammomatoid Ossifying Fibroma Is Defined by *SATB2* Rearrangement

Arjen H.G. Cleven[a,b,*], Karoly Szuhai[c], David G.P. van IJzendoorn[a,d], Eline Groen[a], Hans Baelde[a], Willem H. Schreuder[e], Inge H. Briaire-de Bruijn[a], Stijn W. van der Meeren[f,g], Maarten C. Kleijwegt[h], Wouter R. Furth[i], Herman M. Kroon[j], Albert J.H. Suurmeijer[b], Dilara C. Savci-Heijink[k], Daniel Baumhoer[l], Judith V.M.G. Bovée[a]

[a] *Department of Pathology, Leiden University Medical Center, Leiden, the Netherlands;* [b] *Department of Pathology and Medical Biology, University Medical Center Groningen, University of Groningen, Groningen, the Netherlands;* [c] *Department of Cell and Chemical Biology, Leiden University Medical Center, Leiden, the Netherlands;* [d] *Department of Pathology, Stanford University, Stanford, California;* [e] *Department of Oral and Maxillofacial Surgery/Head and Neck Surgery, Amsterdam University Medical Center/Antoni van Leeuwenhoek Hospital, Amsterdam, the Netherlands;* [f] *Department of Ophthalmology, Leiden University Medical Center, Leiden, the Netherlands;* [g] *Department of Ophthalmology, Amsterdam University Medical Center, Amsterdam, the Netherlands;* [h] *Department Head and Neck Surgery, Leiden University Medical Center, Leiden, the Netherlands;* [i] *Department of Neurosurgery, Leiden University Medical Center, Leiden, the Netherlands;* [j] *Department of Radiology, Leiden University Medical Center, Leiden, the Netherlands;* [k] *Department of Pathology, Academic Medical Center, Amsterdam, the Netherlands;* [l] *Bone Tumour Reference Centre, Institute of Medical Genetics and Pathology, University Hospital Basel, University of Basel, Basel, Switzerland*

ARTICLE INFO

Article history:
Received 11 April 2022
Revised 12 September 2022
Accepted 16 September 2022

Keywords:
juvenile psammomatoid ossifying fibroma
psammomatoid ossifying fibroma
SATB2

ABSTRACT

Psammomatoid ossifying fibroma (PsOF), also known as juvenile PsOF, is a benign fibro-osseous neoplasm predominantly affecting the extragnathic bones, particularly the frontal and ethmoid bones, with a preference for adolescents and young adults. The clinical and morphologic features of PsOF may overlap with those of other fibro-osseous lesions, and additional molecular markers would help increase diagnostic accuracy. Because identical chromosomal breakpoints at bands Xq26 and 2q33 have been described in 3 cases of PsOF located in the orbita, we aimed to identify the exact genes involved in these chromosomal breakpoints and determine their frequency in PsOF using transcriptome sequencing and fluorescence in situ hybridization (FISH). We performed whole RNA transcriptome sequencing on frozen tissue in 2 PsOF index cases and identified a fusion transcript involving *SATB2*, located on chromosome 2q33.1, and *AL513487.1*, located on chromosome Xq26, in one of the cases. The fusion was validated using reverse transcription (RT)-PCR and *SATB2* FISH. The fusion lead to a truncated protein product losing most of the functional domains. Subsequently, we analyzed an additional 24 juvenile PsOFs, 8 juvenile trabecular ossifying fibromas (JTOFs), and 11 cemento-ossifying fibromas (COFs) for *SATB2* using FISH and found evidence of *SATB2* gene rearrangements in 58% (7 of 12) of the evaluable PsOF cases but not in any of the evaluable JTOF ($n = 7$) and COF ($n = 7$) cases. A combination of SATB2 immunofluorescence and a 2-color *SATB2* FISH in our index case revealed that most tumor cells harboring the rearrangement lacked SATB2 expression. Using immunohistochemistry, 65% of PsOF, 100% of JTOF, and 100% of COF cases showed moderate or strong staining for SATB2. In these cases, we observed a mosaic pattern of expression with >25% of the spindle cells in between the bone matrix, with osteoblasts and osteocytes being positive for SATB2. Interestingly, 35% (8 of 23) of PsOFs, in contrast to JTOFs and COFs, showed SATB2 expression in <5% of cells. To our knowledge, this is the first report that shows the involvement of *SATB2* in the development of a neoplastic lesion. In this study, we have showed that *SATB2* rearrangement is a recurrent molecular alteration that appears to be highly specific for PsOF. Our findings support that PsOF is not only morphologically and clinically but also genetically distinct from JTOF and COF.

These authors contributed equally: Arjen H. G. Cleven, Karoly Szuhai, Daniel Baumhoer, and Judith V.M.G. Bovée.

* Corresponding author.
E-mail address: a.h.g.cleven@lumc.nl (A.H.G. Cleven).

0893-3952/$ - see front matter
https://doi.org/10.1016/j.modpat.2022.100013

Introduction

In craniofacial bones, 3 types of ossifying fibromas can be distinguished: cemento-ossifying fibroma (COF); juvenile trabecular ossifying fibroma (JTOF); and psammomatoid ossifying fibroma (PsOF), also known as juvenile psammomatoid ossifying fibroma (JPOF).[1-4] COF is considered a benign odontogenic neoplasm and develops exclusively in the tooth-bearing parts of the jaws. It has a preference to occur in the mandible, favoring the molar and premolar regions in the third to the fourth decade of life with a female predilection.[1-4] JTOF and PsOF most commonly occur in the second decade without predilection for a particular sex; however, they can also develop later in life. PsOF is most common in the periorbital frontal and ethmoid bones, whereas JTOF generally affects the jaws, with the maxilla representing the most prevalent site. JTOF and PsOF can show more rapid growth and expansion, causing facial disfigurement, visual changes, and sinus dysfunction. In contrast, COF usually presents as a well-defined and slowly progressing mass that can reach considerable sizes even if left untreated.[1-4]

Correlating radiological and morphologic findings is essential for the accurate classification of bone tumors. PsOF characteristically shows small, spherical, and paucicellular ossicles (resembling psammomatoid bodies) rimmed by flattened osteoblasts.[1,3,4] However, the morphology of PsOF may overlap with COF, JTOF, or other fibro-osseous lesions, such as fibrous dysplasia, cemento-osseous dysplasia, and low-grade osteosarcoma.

Some studies detected mutations in *CDC73* (HRPT2) in patients with hyperparathyrodism-jaw tumor syndrome.[5] However, in the pathogenesis of sporadic COF, *CDC73* mutations seem to play only a minor role because the reported frequency was only 5%.[6,7] *GNAS* mutations are a frequent (86%) finding in craniofacial fibrous dysplasia, and low-grade osteosarcoma harbors *MDM2* amplifications in 25% to 30% of cases.[6,8,9] In contrast, the molecular pathogenesis of PsOF and JTOF is largely unknown. Identical chromosomal breakpoints at bands Xq26 and 2q33 were described in 3 cases of PsOF located in the orbita.[10,11] Two of the tumors showed an identical t(X;2)(q26;q33) balanced translocation, and the third tumor revealed an interstitial insertion of bands 2q24.2q33 into Xq26 as the sole abnormality.[10,11] We aimed to identify the exact genes involved in these chromosomal breakpoints and determine their frequency in PsOF using transcriptome sequencing and fluorescence in situ hybridization (FISH).

Materials and Methods

Patient Samples

We included 2 PsOF index cases (L6867 and L6605) with available frozen material for RNA sequencing from the Leiden University Medical Center (LUMC). To validate our results using FISH, we included formalin-fixed paraffin-embedded tissue from an additional 25 PsOF cases (22 cases from the University Hospital of Basel, Switzerland; 2 cases from LUMC; and 1 case from University Medical Center Groningen), 8 JTOFs from Basel, and 11 COFs samples from Basel (Table). Most samples were decalcified, and in many cases, the decalcification protocol (time and used reagents) could not be retrieved. All LUMC samples were retrieved from the bone and soft tissue tumor biobank after obtaining informed consent as approved by the LUMC ethical board (B21.022). Ethical approval for the Basel cases was provided by the "Ethikkommission beider Basel" (ref. 274/12). Samples were coded (pseudonymized) according to the Dutch code of proper secondary use of human material as accorded by the Dutch Society of Pathology (Federa).

RNA Sequencing Using Transcriptome Sequencing

RNA was extracted from a fresh frozen tissue sample of L6867 and L6605, obtained after surgery and stored at −80 °C. Approximately 15 slices of 20 μm were cut, after which TRizol (Life Technologies) was added. Nucleotide extraction was performed as described by van IJzendoorn et al,[12] and an additional RNA purification step was included; this step was performed using an RNeasy Mini Kit (Qiagen) following the manufacturer's protocols.

The NEBNext Ultra II Directional RNA Library Prep Kit for Illumina was used to process the samples. Sample preparation was performed according to the protocol "NEBNext Ultra II Directional RNA Library Prep Kit for Illumina" (Illumina, NEB#E7760S/L). Briefly, ribosomal (rRNA) was depleted from total RNA using the rRNA Depletion Kit (Illumina, NEB#E6310). After fragmentation of the rRNA-depleted RNA, complementary DNA (cDNA) synthesis was performed using ligation of the sequencing adapters and PCR amplification. The quality and yield after sample preparation were measured with the Fragment Analyzer. The size of the resulting products was consistent with the expected size distribution (a broad peak between 300 and 500 base pairs). Clustering and DNA sequencing using the NovaSeq6000 were performed according to the manufacturer's protocols, with 50 million paired-end reads of 150 base pairs.

RNA Sequencing Analysis With Defuse

To analyze the transcriptome data of L6867 and L6605, the sequenced reads were aligned to the hg19 reference genome using an in-house pipeline, in which alignment was performed with TopHat2 (v2.0.13) to the hg19 (http://genome.ucsc.edu/) and hg38 reference genomes (http://genome.ucsc.edu/). Fusions were identified using Defuse (v0.6.2) aligning to the hg19 reference genome (http://genome.ucsc.edu/) and filtered with the repeats library from UCSC (http://genome.ucsc.edu/). Subsequently, the identified fusions were sorted according to the number of reads spanning each fusion.

Reverse-transcription PCR

The total RNA of the PsOF index case L6867 was isolated as mentioned earlier, and 1 μg was converted to cDNA. Briefly, the RNA was denatured for 15 minutes at 60 °C and placed on ice. Subsequently, total RNA was added to RNasin (Promega), 5x RT-buffer (Promega), oligodT (Promega), random primer (Promega), dNTPs, and AMV-RT (Roche) enzyme mix and incubated at 42 °C for 1 hour to generate the cDNA. Finally, the RT enzyme was inactivated at 65 °C for 15 minutes. The primers designed for the fusion identified using Defuse included forward primer 5'-TGCGTTTTATTGCGACCTGC-3' (*SATB2*) and reverse primer 5'-GCAGGTGCAGCAGAGTGTTA-3' (*AL513487.1*). PCR was performed using SYBR Green Master Mix (Bio-Rad), with an annealing temperature of 60 °C for 40 cycles. The PCR product was purified with a QIAquick PCR Purification Kit (Qiagen) and further analyzed by Sanger sequencing using the aforementioned primers.

Table
Clinicopathologic characteristics of study cases

Case	Age (y)	Sex	Location	FISH: split/no split in *SATB2*	SATB2 IHC[d]
PsOF_1[L6867]	14	Male	Sinus maxillaris	Split[a,b]	Positive
PsOF_2[L6605]	12	Male	Orbita	Split[a,b,c]	Positive
PsOF_3	12	Female	Orbita	Split[a]	Negative
PsOF_4	11	Male	Orbita	Split[a]	Negative
PsOF_5	34	Male	Mandible	Split[a]	Positive
PsOF_6	9	Female	Mandible	Split[a]	Negative
PsOF_7	76	Male	Sinus maxillaris	Split[b]	Negative
PsOF_8	41	Female	Orbita	No split[a,b]	Failed
PsOF_9	25	Male	Sinus maxillaris	No split[a,b]	Positive
PsOF_10	10	Male	Nose (not further specified)	No split[a,b]	Positive
PsOF_11	4	Male	Sinus maxillaris	No split[a,b]	Positive
PsOF_12	10	Male	Frontal bone	No split[a,b,c]	Positive
PsOF_13	13	Female	Mandible	Failed	Positive
PsOF_14	39	Male	Sinus maxillaris	Failed	Negative
PsOF_15	28	Female	Nose (not further specified)	Failed	Negative
PsOF_16	9	Male	Mandible	Failed	Negative
PsOF_17	37	Female	Maxilla	Failed	Positive
PsOF_18	32	Female	Mandible	Failed	Positive
PsOF_19	46	Male	Orbita	Failed	Positive
PsOF_20	46	Male	Mandible	Failed	Positive
PsOF_21	24	Male	Maxilla	Failed	Negative
PsOF_22	23	Male	Maxilla	Failed	Positive
PsOF_23	67	Female	Ethmoid sinus	Failed	Positive
PsOF_24	8	Female	Mandible	Failed	Positive
PsOF_25	53	Female	Sinus maxillaris	Failed	Positive
PsOF_26	24	Female	Sphenoid bone	Failed	Missing
JTOF_1	4	Male	Maxilla	No split	Positive
JTOF_2	12	Male	Mandible	No split	Positive
JTOF_3	12	Female	Mandible	No split	Positive
JTOF_4	23	Male	Maxilla	No split	Positive
JTOF_5	26	Male	Mandible	No split	Positive
JTOF_6	29	Male	Mandible	No split	Positive
JTOF_7	4	Male	Mandible	No split	Positive
JTOF_8	24	Male	Mandible	Failed	Positive
COF_1	17	Female	Mandible	No split	Positive
COF_2	62	Female	Skull	No split	Positive
COF_3	43	Female	Mandible	No split	Positive
COF_4	26	Female	Mandible	No split	Missing
COF_5	33	Female	Mandible	No split	Positive
COF_6	63	Male	Mandible	No split	Positive
COF_7	8	Male	Maxilla	No split	Positive
COF_8	29	Female	Mandible	Failed	Missing
COF_9	67	Male	Skull	Failed	Positive
COF_10	65	Female	Mandible	Failed	Positive
COF_11	16	Male	Maxilla	Failed	Positive

COF, cemento-ossifying fibroma; FISH, fluorescence in situ hybridization; IHC, immunohistochemistry; JTOF, juvenile trabecular ossifying fibroma; PsOF, psammomatoid ossifying fibroma.

[a] FISH result: SATB2 FISH probe set 1.

[b] FISH result: SATB2 FISH probe set 2.

[c] PsOF_2L6605 12 M Orbita Split1fa2. In this case SATB2 FISH probe set 1 failed, probe set 2 was okay. PsOF_12 10 M Frontal bone. No split1, 2fa. In this case SATB2 FISH probe set 2 failed but probe set 1 was okay.

[d] SATB2 IHC: "Positive" represents weak, moderate, or strong SATB2 staining, with >25% of the spindle cells in between the bone matrix and the osteoblasts lining the bone matrix or within the matrix osteocytes being positive. "Negative" represents <5% of all spindle cells, with osteoblasts or osteoclast showing expression of SATB2 with intensity weak, moderate or strong.

FISH

To detect and verify the translocation as a biomarker for PsOF, a 2-color *SATB2* break-apart FISH was performed on the formalin-fixed paraffin-embedded tissue of all PsOF, JTOF, and COF cases included in this study.

The bacterial artificial chromosomes (BAC) probes for interphase FISH were selected and ordered from BACPAC Resources (https://bacpacresources.org/), in which the first probe set included BAC clones RP11-1012A2 (covering chr2:198,923,555-199,135,875, GRCH38/hg38) and RP11-656D8 (covering chr2:199,704,154-199,873,054, GRCH38/hg38) proximal and distal from the *SATB2* bracketing breakpoints within *SATB2*. A second probe set covered the breaks between *SATB2* and the long-range cis-regulatory element (CRE) in the centromeric gene desert 3' of *SATB2* involved in SATB2-associated syndrome (SAS)[13] and involves BAC clones RP11-606G15 (covering chr2:197,852,082-198,059,609, GRCH38/hg38) and RP11-656D8. A 2-color

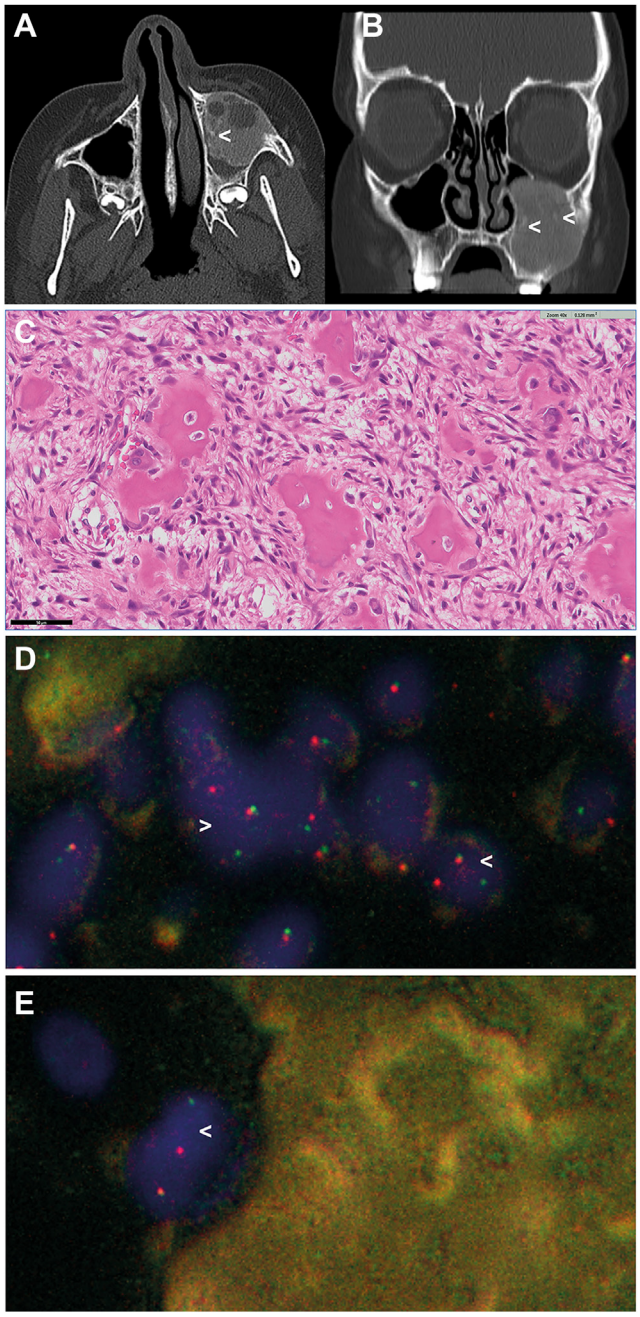

Figure 1.
Radiology, morphology, and *SATB2* fluorescence in situ hybridization (FISH) in psammomatoid ossifying fibroma L6867. (A and B) Axial and coronal reformatted computed tomography images. Inhomogeneous mass in the left maxillary sinus with some expansion and small specs of mineralization (white arrowheads). (C) Typical morphology of psammomatoid ossifying fibroma, with small spherical ossicles (psammomatoid bodies) of bone rimmed with more flattened osteoblasts in a background of a cellular bland-appearing spindle cell component. (D) Case L6867 showing 2 cells (white arrowheads) with a split and a colocalized signal in *SATB2* FISH. (E) Case L6867 showing a split and a colocalized signal in *SATB2* FISH in an osteoblast lining bone matrix (white arrowhead; yellow-green colored).

interphase FISH was set up after labeling the probes with biotin-11dUTP or digoxigenin-11-dUTP (Roche) using a nick translation labeling reaction as described earlier.[14] In these combinations, cases with a translocation involving the *SATB2* gene may directly show a split with both probe sets, whereas cases with the involvement of the CRE may show a split with the second probe set and not with the set bracketing the *SATB2* gene.

Four-micrometer–thick paraffin slides were cut to perform the 2-color FISH as described earlier.[14] In short, slides were pretreated and denatured simultaneously with the probe mixture at 80 °C on a hotplate for 10 minutes. Slides were then incubated in a moist chamber overnight at 37 °C, followed by posthybridization washes and detection of the labeled probes using Cy3-labeled streptavidin (diluted 1:750 in blocking buffer, Sigma-Aldrich) and fluorescein-labeled mouse antidigoxigenin (diluted 1:250 in TNB, Sigma-Aldrich), followed by fluorescein-labeled rabbit anti-mouse diluted at 1:1000 in blocking buffer (Sigma-Aldrich). Slides were embedded with DAPI/Vectashield (Vectorlabs) solution. The slides were scanned using the Pannoramic 250 Flash II slide scanner (3DHistech) and scored using the Pannoramic CaseViewer software (3DHistech) (by K.S., E.G., and A.H.G.C.). Cases were considered positive when >20% of the 100 counted nuclei harbored a split in *SATB2*.

Correlative SATB2 Immunofluorescence and Fluorescence In Situ Hybridization

To correlate SATB2 protein expression patterns in neoplastic cells of the index case, immunofluorescence detection of SATB2 was followed by interphase FISH for SATB2 using digital correlative microscopy after scanning the slides at each round. For the antigen retrieval, 0.1 M citrate (pH = 6.0) solution was used. The primary mouse immunoglobulin G1 SATB2 antibody (Clone CL0276, Invitrogen) and 1:10 in phosphate-buffered saline/bovine serum albumin (1%) were placed on the slide and incubated overnight at 4 °C. The primary antibody was detected using a goat anti-mouse Alexa 594 dye (Invitrogen) diluted at 1:200, followed by incubation with Alexa Fluor 594 donkey anti-goat antibody diluted at 1:500 (Invitrogen). Finally, the slides were mounted with DAPI Citifluor (Citifluor). The slides were scanned with a Pannoramic Flash 250II scanner (3DHistech). After scanning the slide, the cover glass was removed by a phosphate-buffered saline wash, and FISH and scanning were performed according to the aforementioned FISH protocol. The immunofluorescence and FISH results were examined side-by-side to determine whether SATB2 expression was accompanied by the presence or absence of a break-apart of SATB2 in the 100 counted nuclei using the Pannoramic CaseViewer software (3DHistech) (by K.S. and E.G.).

SATB2 Immunohistochemistry

Immunohistochemistry (IHC) was performed on PsOF, JTOF, and COF (n = 44) to determine SATB2 expression using a mouse anti-SATB2 antibody (diluted 1:10) (Clone CL0276, Sigma-Aldrich). IHC was performed using the EnVision FLEX protocol for the Dako Autostainer with the Dako Autostainer Omnis 2x (Agilent) using the EnVision FLEX, high Ph (Dako Omnis), HRP detection kit, Target Retrieval solution, Haematoxylin and Lilies modification by Agilent. Lastly, the slides were dehydrated and mounted using the Dako Coverslipper (Agilent). The slides were assessed independently by 2 bone and soft tissue pathologists (A.H.G.C. and D.B.), and only nuclear staining was considered positive. In discordant cases (n = 4), consensus was reached after discussion. Staining intensity was scored considering the spindle cells in the background, osteoblasts lining the ossicles, and osteocytes (0 = negative, 1 = weak, 2 = moderate, and 3 = strong). The overall percentage of positive nuclei was scored as 0% for a staining intensity of 0, 1% to 24% for a staining intensity of 1, 25% to

49% for a staining intensity of 2, 50% to 74% for a staining intensity of 3, and 75% to 100% for a staining intensity of 4.

After scoring, we observed 2 distinct groups: one group with only a few SATB2-positive cells (overall <5%), which we considered negative for further analysis, and a second group with weak, moderate, or strong scoring in >25% of cells, which we considered positive.

Results

Clinicopathologic Characteristics of PsOF Cases

The first index case (L6867) was a 14-year-old boy who presented with an expansile and inhomogeneous mass in his left maxillary sinus (Fig. 1A, B). Histology showed typical findings of a PsOF, with small spherical ossicles (psammomatoid bodies) of bone surrounded by osteoblast-like cells in a background of a fibroblastic-appearing spindle cell proliferation without cellular atypia. (Fig. 1C).

The second index case (L6605) was a 12-year-old boy with a well-demarcated ossifying lesion arising from the orbital roof on the left and with a close relationship with the ethmoid sinus (Supplementary Fig. S1A). The histologic findings in this case were identical to those in case L6867 (Supplementary Fig. S1B).

In total, 26 cases of PsOF were included in the study, with ages ranging from 4 to 76 years, of which 38% (10 of 26) patients were aged <20 years. Fifteen patients with PsOF were male; 16 cases were located in the gnathic bones and 10 cases were located in the extragnathic bones (including ethmoid, orbita, sphenoid, and nasal bone) (Table).

SATB2-AL513487 Fusion in PsOF L6867 Lead to a Truncated Protein

In the first PsOF index case (L6867), Defuse analysis identified a *SATB2-AL513487* fusion. The chromosomal location of these 2 genes (*SATB2* is located on chromosome 2q33.1 and AL513487.1 is located on chromosome Xq26) matched with the breakpoints of the balanced translocation t(X;2)(q26;q33) and the direct insertion that was described previously in PsOF.[10,11]

The fusion breakpoint was found in exon 3 according to ENST00000417098.6 as reference. The exon numbering might differ between the different transcript variants derived from different promoters. The fusion was validated by RT-PCR (Fig. 2) with the fusion breakpoint in *SATB2*. In silico translation of the sequence showed a 57 amino acid (AA)–long extension and a stop codon. The extended AA sequence did not show similarity to known protein functional domains. After fusion, the first 115 AAs of the 733 AA–long SATB2 protein remained. The deletion led to a loss of the CUT1, CUT2, CUT-like, and homeodomain domains and a partial loss of the ubiquitin ligation domain (AA-60-155) after AA 115. Sanger sequencing verified that the reconstructed sequence can be found in the National Center for Biotechnology Information database with the BankIt2549397 BSeq#1 OM752138 ID.

The second index case (L6605) showed neither fusion nor point mutation involving the *SATB2* gene. However, FISH involving the CRE showed a split in the region, indicating the involvement of the long-range CRE of *SATB2*.

Recurrent SATB2 Break in PsOFs

In 7 of 12 PsOF cases that were suitable for FISH analysis, we detected a split signal for *SATB2*. In PsOF cases with a positive *SATB2* FISH, the density of cells in which we detected the split signal was highly variable between regions within the same tumor (range, 30%-80%). A split signal was observed in the spindle cells in between the bone matrix and the osteoblasts lining the bone matrix (Fig. 1D, E and Table). Five of the *SATB2* FISH-positive cases showed a break with probe set 1, and 2 cases (including index case L6605) showed a split signal only in probe set 2, indicating the involvement of long-range CRE (Table).

We did not observe a *SATB2* break in JTOF (n = 7) or COF (n = 9) that was amenable to FISH analysis (Table)

Loss of SATB2 Expression in PsOF Index Case L6867

SATB2 immunofluorescence and subsequent FISH analysis for *SATB2* were performed in the index case L6867 using the same slide and digital correlative fluorescence microscopy to relocate identical regions from the 2 experiments (Fig. 3 A-C). The results showed that scorable cells harboring a split signal (Fig. 3C) lacked expression of SATB2 (Fig. 3B). Cells that expressed SATB2 showed no split in the *SATB2* FISH (Fig. 3B, C).

SATB2 Immunohistochemical Findings

Using SATB2 IHC, a mosaic pattern identical to the pattern shown using immunohistochemical findings (IFs) in L6867 observed. Overall, SATB2-positive staining was seen in 65% (15 of 23) of PsOF cases (Table). All positive cases showed a variable, heterogeneous, mosaic pattern of moderate to strong SATB2 staining in >25% of the spindle cells in the background, the osteoblasts lining the ossicles, and/or the osteocytes (Fig. 4A).

Interestingly, 8 out of 23 PsOF cases only showed SATB2 staining occasionally in some spindle cells (<5%), with most of the spindle cells as well as osteoblasts and osteoclasts in the psammomatoid bodies being negative for SATB2 (Fig. 4B). Four of these 8 SATB2-negative PsOF cases showed a *SATB2* rearrangement using FISH (Table).

In JTOF (n = 8) and COF (n = 11), all tumors showed diffuse strong nuclear expression in >25% of the cells (Supplementary Fig. S1C, D).

Discussion

PsOF, also known as JPOF, is a benign fibro-osseous neoplasm that predominantly affects the extragnathic bones, particularly the frontal and ethmoid bones, with a preference for adolescents and young adults. The World Health Organization Head and Neck Tumours 2022 edition introduced the term PsOF instead of JPOF because of the wider age range of patients, which was also observed in the current study cohort of PsOF.

Because clinicopathologic features may overlap with those of other fibro-osseous lesions and additional molecular markers are currently lacking, a definitive diagnosis can be challenging, particularly in core needle biopsies. Here, we report the findings of a recurrent *SATB2* rearrangement in >50% of the PsOF cases, which was absent in other ossifying fibromas, including JTOF and COF.

With transcriptome sequencing, we analyzed 2 PsOF cases; of which, 1 case showed *SATB2-AL513487.1* fusion. The *AL513487.1* gene encodes for a predicted noncoding RNA. Our SATB2 IF results suggest that tumor cells with a *SATB2* split show a loss in SATB2 protein expression. For instance, a giant cell tumor of the bone is composed of a heterogeneous population of stromal cells with

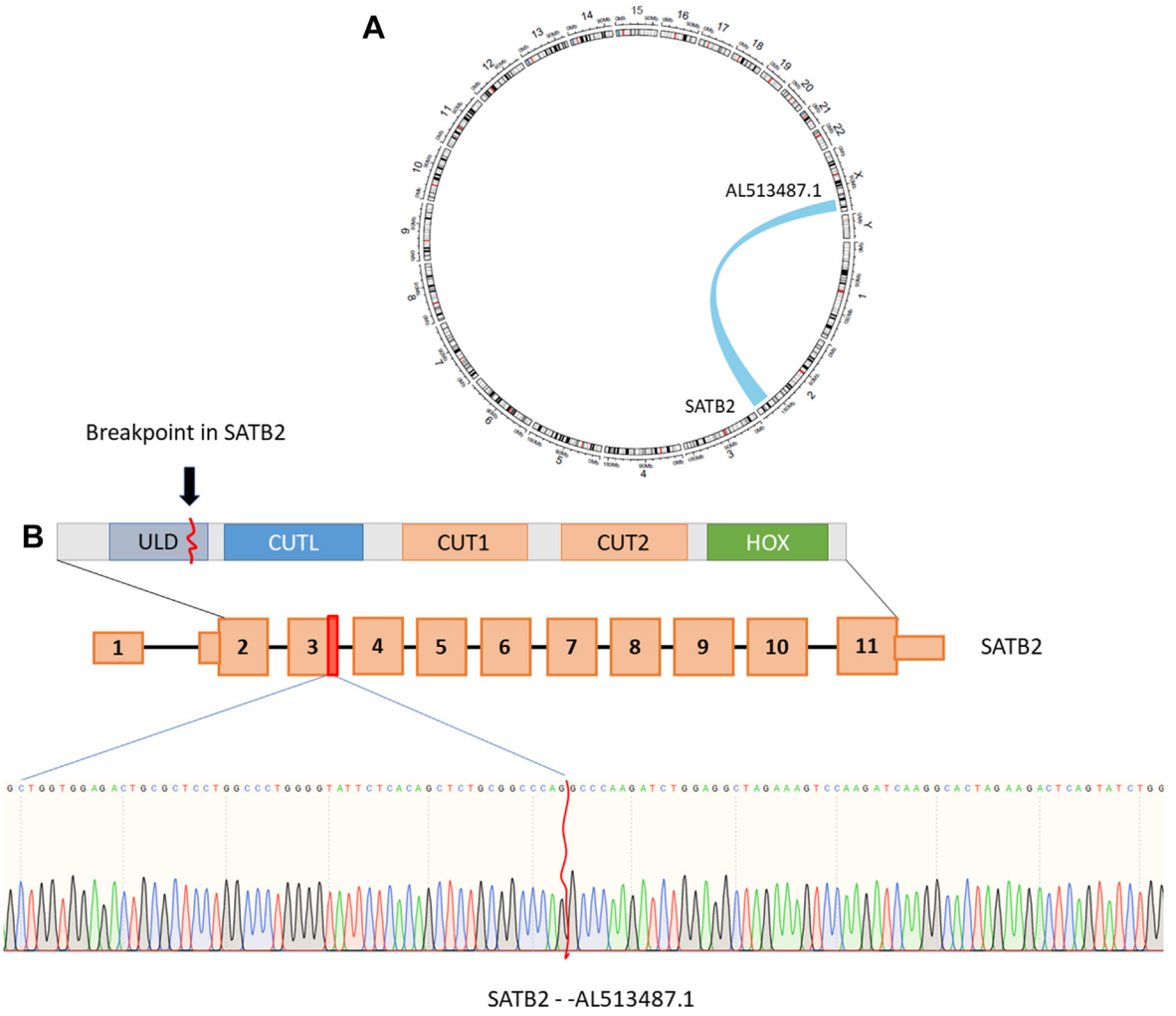

Figure 2.
Fusion between *SATB2* and *AL513487*.1 in psammomatoid ossifying fibroma L6867. (A) Fusion gene map showing the identified gene fusion of *SATB2*, located on chromosome 2q33.1, and *AL513487.1*, located on chromosome Xq26. (B) Reverse-transcription PCR results demonstrating that the breakpoint (red curved line) in *SATB2* is located in exon 3. The exact breakpoint of *AL513487.1* could not be determined because of repetitive sequences in the gene. The first functional domain of *SATB2*, the ubiquitin-like domain (ULD), starts in exon 3. CUTL, CUT-like; HOX, homeodomain.

H3F3A driver mutation and reactive stromal cells without the mutation. Similarly, the SATB2-positive cells in PsOF that lack a split signal in *SATB2* FISH probably represent a reactive cell population.

The index case (L6867) showed a truncation of SATB2, losing several functional domains. It should be noted that the epitope recognition site of the used IHC and IF antibodies cover the region in the lost domains, explaining and supporting the negative staining pattern. Furthermore, on the basis of the IFs, 4 of 7 PsOF cases with *SATB2* rearrangement were considered mostly negative for SATB2.

The *SATB2* gene lies in a gene-poor region on 2q33.1 and codes for the SATB2 protein, an 82.5 kDa protein composed of 733 AAs. In a zebrafish model, SATB2 played an important role in development and tissue regeneration, particularly in craniofacial bone development, osteoblast differentiation, and maturation.[15] The SATB2 protein, a matrix-associated region–binding protein, is part of the CUT superclass of homeodomain proteins, in which *SATB2* consists of 2 CUT domains, one CUT-like domain and a homeodomain domain.[16,17] It binds to matrix-associated regions, thereby activating or repressing transcription because it can influence the interplay between enhancers and promoters and regulate chromatin structures.[18] SATB2 is known to downregulate certain *HOX* genes, and it regulates the transcription factors involved in osteoblast differentiation, such as RUNX2 (runt-related transcription factor) and ATF (cyclic adenosine monophosphate-dependent transcription factor).[18]

Several single nucleotide variants (SNVs) and various sizes of deletions, including multiple exons and translocations involving the *SATB2* gene, have been reported in the context of (isolated) cleft palate and SAS (OMIM #612313, also known as Glass syndrome).[16] This syndrome is characterized by impaired neurodevelopment and craniofacial anatomical aberrations.[16-18]

SATB2 expression is strongly regulated by long-range CREs, as identified in the context of SAS.[17] Interestingly, balanced translocations leading to the disruption of the 3' long-range CRE have been reported.[13,16,17] Furthermore, balanced autosomal translocations t(2;7)(q33;p21) and t(2;11)(q32;p14) have been

described in SAS, and disruption of the coding region of the *SATB2* gene between exon 2 and 3 resulted in an isolated cleft palate phenotype in these patients; however, no fibro-osseous lesions have been reported.[13,15,16,19] The breakpoints in SAS are comparable with the breakpoint we observed in our PsOF cases. In all reported cases, the disruption of SATB2 lead to a dominant-negative effect on the function of SATB2 protein, including the CRE.[13,15-17]

To our knowledge, our report is the first to identify the direct structural involvement of SATB2 protein in the development of a tumor with an intriguing overlap in the anatomical site of tumor appearance and syndromic involvement of the gnathic bones in affected individuals with SAS.

We described a recurrent translocation in 7 cases, including 2 cases in which the disruption likely involved the 3'-CRE as identified by interphase FISH. One of these 2 cases was the index case L6605, which involved the CRE domain and for which transcriptome sequencing did not show an SNV or fusion.

In the remaining FISH-negative cases with or without SATB2 IHC positivity, we could not exclude the possibility of inactivating SNVs in the *SATB2* gene, similar to what has been described as a frequent event in SAS.[17] Seemingly, these inactivating mutations lead to a dominant inactivation of *SATB2*, resulting in the syndromic appearance by a mechanism that is not yet not fully understood.

In a recent article, Toferer et al[20] reported a frameshift somatic mutation in the *SETD2* gene in a 21-year-old man with a PsOF and secondary aneurysmal bone cyst-like changes in the mandible. The *SETD2* gene is located on chromosome 3p21.31 and encodes a histone methyltransferase, which is responsible for the trimethylation of lysine 36 of histone H3. Mutations of the *SETD2* gene have been found in a variety of malignant tumors, including pancreatic and renal carcinomas.[20] Whether *SETD2* mutations are a recurrent genetic finding in PsOF remains to be elucidated because this was detected only in 1 case of PsOF. We did not find evidence of *SETD2* mutation in our PsOF index cases L6867 and L6605.

In conclusion, we have shown that *SATB2* rearrangements are a recurrent molecular genetic alteration that seems specific to PsOF. Based on our results, PsOF is not only morphologically and clinically but also genetically distinct from JTOF and COF. Although

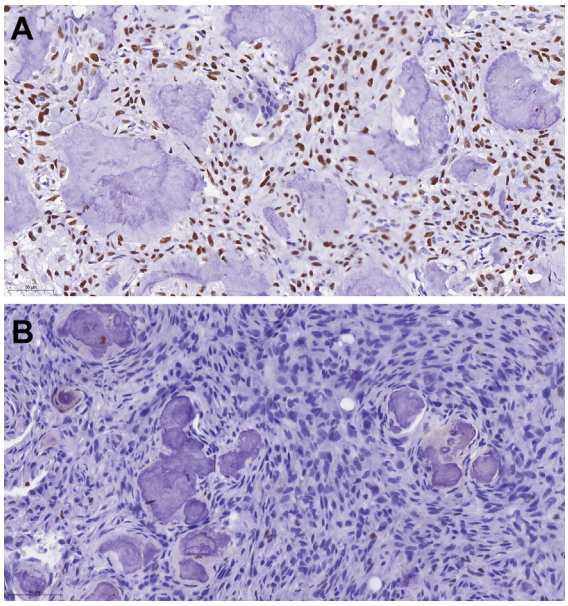

Figure 4.
SATB2 expression using immunohistochemistry in psammomatoid ossifying fibroma (PsOF) cases. (A) Strong SATB2 nuclear expression in the majority (> 25%) of the spindle cells (PsOF index case L6867), with SATB2 positive osteoblasts and osteocytes surrounding and in the spherical ossicles. (B) Focally (<5%) weak SATB2 expression in the spindle cell proliferation; most of the spindle cells, osteoblasts, and osteocytes were SATB2 negative (PsOF case 3, see the Table, *SATB2* fluorescence in situ hybridization positive). Scale bars = 50 μm.

SATB2 FISH can be used as a diagnostic tool for PsOF, the exact role of *SATB2* rearrangement in the etiology of PsOF requires further research, which may shed light on the developmental biology and bone physiology as well as the involvement of *SATB2* in SAS.

Author Contributions

A.H.G.C. initiated the study and collected and analyzed the data. E.G., and H.B. collected data for fluorescence in situ

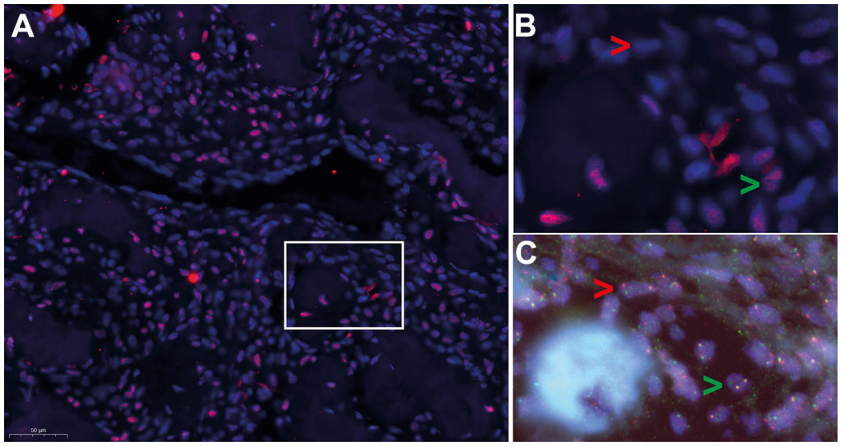

Figure 3.
SATB2 expression using immunofluorescence in psammomatoid ossifying fibroma L6867. (A) SATB2 IFs demonstrated a mosaic pattern of cells with (purple) and without SATB2 expression (blue) scattered between the bone matrix (scale bar = 50 μm). (B) The combined images on high power in a specific area (white square in Fig. 3A) of the SATB2 IF. (C) Two-colored fluorescence in situ hybridization results showing cells harboring the translocation lack SATB2 expression (red arrowheads in Fig. 3B, C), and cells without the translocation exhibit SATB2 expression (green arrowheads in Fig. 3B, C).

hybridization. W.H.S. S.W.v.d.M., M.C.K., W.R.F., A.J.H.S., and D.C.S.-H. collected patient material. D.B. collected the Basel cohort data and samples. K.S. supervised the methodology. H.M.K. acquired the radiology images. J.V.M.G.B. conducted the experimental planning. I.H.B.B. performed RNA isolation and immunohistochemistry. D.B. performed immunohistochemistry scoring. K.S. and D.G.P.v.I. analyzed the data. J.V.M.G.B. supervised the study. A.H.G.C. wrote the manuscript with contributions from K.S., D.B., and J.V.M.G.B.

Data Availability

No data are available to the public. All data are stored at the Department of Pathology, Leiden University Medical Center, Leiden, the Netherlands.

Funding

This study was funded by the International Skeletal Society 2019-2020 Seed Grant.

Declaration of Competing Interests

All authors have no conflict of interest.

Ethics Approval and Consent to Participate

All Leiden University Medical Center samples were retrieved from the bone and soft tissue tumor biobank after informed consent was obtained as approved by the Leiden University Medical Center ethical board (B21.022). Ethical approval for the Basel cases was provided by the “Ethikkommission beider Basel” (ref. 274/12). Samples were coded (pseudonymized) according to the Dutch code of proper secondary use of human material as accorded by the Dutch Society of Pathology (Federa).

Supplementary Material

The online version contains supplementary material available at https://doi.org/10.1016/j.modpat.2022.100013.

References

1. Adel K, El-Naggar JKCC, Grandis JR, Takata T, Slootweg PJ, eds. *WHO Classification of Head and Neck Tumours*. 4th ed. IARC Publications; 2017.
2. Slootweg P. Pathology of the maxillofacial bones. A guide to diagnosis. In: *Pathology of the Maxillofacial Bones. A Guide to Diagnosis*. Springer International Publishing; 2015:5–6.
3. Slootweg PJ. Juvenile trabecular ossifying fibroma: an update. *Virchows Arch*. 2012;461(6):699–703.
4. Slootweg PJ, Panders AK, Koopmans R, Nikkels PG. Juvenile ossifying fibroma. An analysis of 33 cases with emphasis on histopathological aspects. *J Oral Pathol Med*. 1994;23(9):385–388.
5. Ciuffi S, Cianferotti L, Nesi G, et al. Characterization of a novel *CDC73* gene mutation in a hyperparathyrodism-jaw tumor patient affected by parathyroid carcinoma in the absence of somatic loss of heterozygosity. *Endocr J*. 2019;66(4):319–327.
6. Cleven AHG, Schreuder WH, Groen E, Kroon HM, Baumhoer D. Molecular findings in maxillofacial bone tumours and its diagnostic value. *Virchows Arch*. 2020;476(1):159–174.
7. Chen Y, Hu DY, Wang TT, et al. *CDC73* gene mutations in sporadic ossifying fibroma of the jaws. *Diagn Pathol*. 2016;11(1):91.
8. Shi RR, Li XF, Zhang R, Chen Y, Li TJ. *GNAS* mutational analysis in differentiating fibrous dysplasia and ossifying fibroma of the jaw. *Mod Pathol*. 2013;26(8):1023–1031.
9. Lopes MA, Nikitakis NG, Ord RA, Sauk Jr J. Amplification and protein expression of chromosome 12q13-15 genes in osteosarcomas of the jaws. *Oral Oncol*. 2001;37(7):566–571.
10. Parham DM, Bridge JA, Lukacs JL, Ding Y, Tryka AF, Sawyer JR. Cytogenetic distinction among benign fibro-osseous lesions of bone in children and adolescents: value of karyotypic findings in differential diagnosis. *Pediatr Dev Pathol*. 2004;7(2):148–158.
11. Sawyer JR, Tryka AF, Bell JM, Boop FA. Nonrandom chromosome breakpoints at Xq26 and 2q33 characterize cemento-ossifying fibromas of the orbit. *Cancer*. 1995;76(10):1853–1859.
12. van IJzendoorn DG, de Jong D, Romagosa C, et al. Fusion events lead to truncation of FOS in epithelioid hemangioma of bone. *Genes Chromosomes Cancer*. 2015;54(9):565–574.
13. Rainger JK, Bhatia S, Bengani H, et al. Disruption of SATB2 or its long-range cis-regulation by SOX9 causes a syndromic form of Pierre Robin sequence. *Hum Mol Genet*. 2014;23(10):2569–2579.
14. Rossi S, Szuhai K, Ijszenga M, et al. *EWSR1-CREB1* and *EWSR1-ATF1* fusion genes in angiomatoid fibrous histiocytoma. *Clin Cancer Res*. 2007;13(24):7322–7328.
15. Pradhan SJ, Reddy PC, Smutny M, et al. Satb2 acts as a gatekeeper for major developmental transitions during early vertebrate embryogenesis. *Nat Commun*. 2021;12(1):6094.
16. FitzPatrick DR, Carr IM, McLaren L, et al. Identification of *SATB2* as the cleft palate gene on 2q32-q33. *Hum Mol Genet*. 2003;12(19):2491–2501.
17. Zarate YA, Bosanko KA, Caffrey AR, et al. Mutation update for the *SATB2* gene. *Hum Mutat*. 2019;40(8):1013–1029.
18. Dobreva G, Chahrour M, Dautzenberg M, et al. SATB2 is a multifunctional determinant of craniofacial patterning and osteoblast differentiation. *Cell*. 2006;125(5):971–986.
19. Huang X, Chen Q, Luo W, et al. SATB2: A versatile transcriptional regulator of craniofacial and skeleton development, neurogenesis and tumorigenesis, and its applications in regenerative medicine. *Genes Dis*. 2022;9(1):95–107.
20. Toferer A, Truschnegg A, Kashofer K, Beham-Schmid C, Beham A. First presentation of a frameshift mutation in the *SETD2* gene of a juvenile psammomatoid ossifying fibroma (JPOF) associated with an aneurysmal bone cyst. *Diagn Pathol*. 2021;16(1):91.